

Quantifying the Uncertainty in the Coefficient of Restitution Obtained with Accelerometer Data from a Crash Test

Nathan A. Rose
Gray Beauchamp
Will Bortles
Kineticorp, LLC

Copyright © 2007 SAE International

ABSTRACT

This paper details a method for obtaining the coefficient of restitution from a vehicle-to-vehicle crash test and for quantifying the uncertainty in the resulting value. The coefficient of restitution is determined by analyzing accelerometer data to obtain the post-impact velocity conditions for the test and, by then, using the method of least squares to fit an impulse-momentum solution to the results of the accelerometer data analysis.

Uncertainties that affect the accelerometer data analysis include uncertainties associated with the acceleration readings and the accelerometer locations within the vehicle-fixed coordinate system. Uncertainties that affect the fit between the impulse-momentum solution and the post-impact velocity conditions include uncertainty associated with the vehicle weights and moments of inertia and uncertainty associated with the placement of the impact center. Also, since uncertainties in the accelerometer data analysis result in a range of values for the post-impact velocity conditions, there is a range of possible matches between the accelerometer data analysis and the impulse-momentum equations.

This paper presents a case study for which the combined effects of uncertainty from the accelerometer data analysis and the fitting of this analysis with an impulse-momentum solution are quantified. A general method is presented for quantifying the uncertainty in the analysis of the coefficient of restitution for any particular crash test.

INTRODUCTION

The following steps will yield the coefficient of restitution for a vehicle-to-vehicle crash test. First, obtain the crash test report, video footage, and signals from at least two vehicle-mounted accelerometers per vehicle. For crash tests conducted for the National Highway Traffic Safety Administration (NHTSA), much of this data is available

from NHTSA's research and development website (<http://www-nrd.nhtsa.dot.gov>). Select signals from accelerometers attached to portions of the vehicle isolated from the crushing region of each vehicle. Use vehicle weights, dimensions, crush measurements, photographs, and reported accelerometer positions from the test report to diagram the impact configuration for the test, to determine the location of each vehicle's center of mass (CoM), and to locate the accelerometers for each vehicle relative to the CoM. To complete these steps, the vehicle data contained in the test report may need to be supplemented with additional specifications obtained from other sources.

Next, filter the accelerometer signals and, then, analyze them in accordance with the equations presented in References 1, 2, and 3. These equations will yield the vehicles' translational and angular velocities throughout the impact. These, in turn, can be used to obtain the CoM change in velocity (ΔV), the post-impact yaw velocity, and the post-impact velocity direction for each vehicle. The relevant equations from these publications are included in the "Accelerometer Data Analysis" section below.

Based on the impact configuration diagram and crush profiles, determine the orientation of the intervehicular contact surface and then estimate the impact center location for the impact. The impact center is the point at which the resultant collision force is transferred during the impact. Finally, apply the equations of planar impact mechanics (pim) to determine the coefficient of restitution for each test [4]. Within the planar impact mechanics analysis, use the method of least squares to optimize the impact center location, impulse ratio, and coefficient of restitution to obtain the best possible match with the ΔV s, post-impact yaw velocities and post-impact velocity directions determined from the accelerometer data analysis [5]. Once the best fit match is obtained, the coefficient of restitution from this optimization can be considered the coefficient of restitution for the crash test.

ACCELEROMETER DATA ANALYSIS

References 1, 2 and 3 present equations from which a vehicle's CoM ΔV , post-impact velocity magnitude and direction, and its post-impact yaw velocity can be obtained based on data from two accelerometers located at known points on the vehicle. These equations are given below in Equations (1), (17), (18), (19), (24), (25), (30) and (31). The reader is referred to these references for a full treatment of these equations.

Figure 1 shows the orientation of the vehicle-fixed coordinate system used for many crash tests. This figure also shows the location of two accelerometers, **a** and **b**, located relative to the vehicle CoM with the vectors r_a and r_b . Given this vehicle-fixed coordinate system and the position vectors r_a and r_b , the following equation yields the vehicle's yaw acceleration based on signals from accelerometers **a** and **b**:

$$\alpha = \frac{(a_{ax} - a_{bx})(r_{by} - r_{ay}) - (a_{ay} - a_{by})(r_{bx} - r_{ax})}{(r_{bx} - r_{ax})^2 + (r_{by} - r_{ay})^2} \quad (1)$$

In Equation (1), a_{ax} and a_{ay} are the x and y direction accelerations at accelerometer **a**, a_{bx} and a_{by} are the x and y direction accelerations at accelerometer **b**, and r_{ax} , r_{ay} , r_{bx} , and r_{by} are the longitudinal and lateral coordinates of accelerometers **a** and **b** relative to the vehicle CoM.

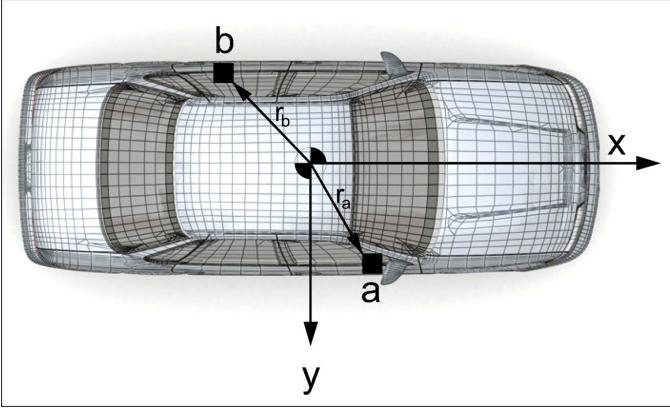


Figure 1 – Vehicle-Fixed Coordinate System with Accelerometer Locations

The uncertainty in the angular acceleration of Equation (1) can be written as follows [6, 7, 8]:

$$\delta\alpha = \sqrt{A^2 \delta a_{ax}^2 + B^2 \delta a_{bx}^2 + C^2 \delta a_{ay}^2 + D^2 \delta a_{by}^2 + E^2 \delta r_{by}^2 + F^2 \delta r_{ay}^2 + G^2 \delta r_{bx}^2 + H^2 \delta r_{ax}^2} \quad (2)$$

In Equation (2), the variations, δa_{ax} , δa_{bx} , δa_{ay} , δa_{by} , δr_{by} , δr_{ay} , δr_{bx} , and δr_{ax} , represent the uncertainties in the measured values of a_{ax} , a_{bx} , a_{ay} , a_{by} , r_{by} , r_{ay} , r_{bx} , and r_{ax} .

The variables A through H are referred to as the sensitivity coefficients and are defined by Equations (3) through (10).

$$A = \frac{\partial \alpha}{\partial a_{ax}} = \frac{r_{by} - r_{ay}}{(r_{bx} - r_{ax})^2 + (r_{by} - r_{ay})^2} \quad (3)$$

$$B = \frac{\partial \alpha}{\partial a_{bx}} = -A \quad (4)$$

$$C = \frac{\partial \alpha}{\partial a_{ay}} = -\frac{r_{bx} - r_{ax}}{(r_{bx} - r_{ax})^2 + (r_{by} - r_{ay})^2} \quad (5)$$

$$D = \frac{\partial \alpha}{\partial a_{by}} = -C \quad (6)$$

$$E = \frac{\partial \alpha}{\partial r_{by}} = (a_{ax} - a_{bx})(D^2 - A^2) + 2(a_{ay} - a_{by})AD \quad (7)$$

$$F = \frac{\partial \alpha}{\partial r_{ay}} = -E \quad (8)$$

$$G = \frac{\partial \alpha}{\partial r_{bx}} = (a_{ay} - a_{by})(D^2 - A^2) - 2(a_{ax} - a_{bx})AD \quad (9)$$

$$H = \frac{\partial \alpha}{\partial r_{ax}} = -G \quad (10)$$

The uncertainty in the accelerometer positions for a particular crash test will depend on the method used to measure their location. Assuming that a particular test facility employs a consistent methodology, the uncertainties in the accelerometer locations will be independent of the coordinate direction and the specific accelerometer, so that $\delta r_{by} = \delta r_{ay} = \delta r_{bx} = \delta r_{ax} = \delta r$. The acceleration uncertainties cannot be simplified in this same way, since, in general they will vary from accelerometer to accelerometer and from coordinate direction to coordinate direction. Equation (2) can, therefore, be written as follows:

$$\delta\alpha = \sqrt{A^2(\delta a_{ax}^2 + \delta a_{bx}^2) + C^2(\delta a_{ay}^2 + \delta a_{by}^2) + 2(E^2 + G^2)\delta r^2} \quad (11)$$

In the analysis that follows, the acceleration uncertainties for each channel will be stated as a fixed percentage of the full-scale value. Thus, in Equation (11), E and G will be the only non-constant terms.

Integration of Equation (1) yields the vehicle's yaw velocity. By examining Equations (1) through (11), several observations can be made that are relevant to

assessing the uncertainties that will propagate through this integration into the calculated yaw velocity. First, the yaw acceleration depends on the longitudinal and lateral distances between accelerometers **a** and **b**, not the accelerometers absolute position relative to the vehicle CoM. In Equations (1) through (11), these distances are assumed constant and their signs depend on the quadrants in which the accelerometers are located.

Second, when $r_{bx} \approx r_{ax}$ and $r_{by} \approx r_{ay}$, the denominator of Equation (1) will become very small and the sensitivity coefficients A through D will become large. In this case, Equation (1) will exhibit excessive sensitivity to the uncertainties in the accelerometer positions and the acceleration readings. Since the denominator of Equation (1) is the square of the distance between the accelerometers, Equation (1) will be least sensitive to measurement uncertainties when the distance between the accelerometers is maximized. The distance between accelerometers can, therefore, be used as a quantitative tool for judging between two possible accelerometer combinations.

Finally, the sensitivity coefficients for the acceleration uncertainties, Equations (3) through (6), are inversely proportional to the square of the distance separating the accelerometers. The sensitivity coefficients for the position uncertainties, Equations (7) through (10), are inversely proportional to the distance separating the accelerometers, raised to the fourth power. Thus, in general, the sensitivity coefficients related to the positional uncertainties will be of smaller magnitude than those related to the acceleration uncertainties and the analysis will be more sensitive to the acceleration uncertainties than the positional uncertainties.

To quantify the propagation of uncertainty from the yaw acceleration, $\delta\alpha$, into the yaw velocity, consider the following equation, which represents integration of the yaw acceleration using the Trapezoid Rule:

$$\omega_t = \omega_{t-\Delta t} + \frac{\Delta t}{2} [\alpha_{t-\Delta t} + \alpha_t] \quad (12)$$

Equation (12) yields the yaw velocity at time t based on the yaw velocity at the prior time step, t-Δt, and the yaw acceleration at times t and t-Δt. The uncertainty associated with Equation (12) can be written as follows:

$$\delta\omega_t = \delta\omega_{t-\Delta t} + \sqrt{\left(\frac{\partial\omega_t}{\partial\alpha_{t-\Delta t}}\right)^2 \delta\alpha_{t-\Delta t}^2 + \left(\frac{\partial\omega_t}{\partial\alpha_t}\right)^2 \delta\alpha_t^2} \quad (13)$$

Equation (13) accounts for the uncertainty that accrues in the integration due to uncertainty in the discrete values of the angular acceleration. It does not account for the discretization error inherent in the integration. For the analysis carried out later in this paper, the magnitude

of the discretization error was examined [6] and it was found to be negligible relative to the effects of the uncertainty in the discrete angular acceleration values. This being the case, the discretization error is not discussed here.

After evaluating the partial derivatives, Equation (13) can be rewritten as follows:

$$\delta\omega_t = \delta\omega_{t-\Delta t} + \frac{\Delta t}{2} \sqrt{\delta\alpha_{t-\Delta t}^2 + \delta\alpha_t^2} \quad (14)$$

Integrating the angular velocity data from Equation (12) yields the vehicle heading angle. Analogous to Equation (12), Equation (15) gives a Trapezoid Rule integration of the angular velocity.

$$\theta_t = \theta_{t-\Delta t} + \frac{\Delta t}{2} [\omega_{t-\Delta t} + \omega_t] \quad (15)$$

Analogous to Equation (14), Equation (16) yields the uncertainty in Equation (15).

$$\delta\theta_t = \delta\theta_{t-\Delta t} + \frac{\Delta t}{2} \sqrt{(\delta\omega_{t-\Delta t})^2 + (\delta\omega_t)^2} \quad (16)$$

Thus, Equations (11), (14), and (16) yield the uncertainty in the calculated yaw acceleration, yaw velocity, and heading angle when we rely on Equations (1), (12), and (15) to calculate these quantities.

In addition to Equation (1), the following equation is also used to obtain the vehicles' CoM accelerations:

$$\omega^2 = \frac{(a_{ax} - a_{bx})(r_{bx} - r_{ax}) + (a_{ay} - a_{by})(r_{by} - r_{ay})}{(r_{bx} - r_{ax})^2 + (r_{by} - r_{ay})^2} \quad (17)$$

As with Equation (1), Equation (17) depends on the distance between accelerometers **a** and **b**, not the accelerometers absolute position relative to the vehicle CoM. The denominator of Equation (17) is also identical to the denominator of Equation (1) and, thus, sensitivity in Equation (17) will also be minimized by selecting accelerometers that are as far apart as practical. Using the same technique as that used above, it can be shown that the uncertainty in Equation (17) is equal to the uncertainty in Equation (1). Thus, Equation (11) also characterizes the uncertainty in Equation (17).

The following equations yield the CoM x and y direction accelerations in the vehicle-fixed coordinate system:

$$a_{c_{gx}} = \frac{1}{2} (a_{ax} + a_{bx} + \alpha(r_{ay} + r_{by}) + \omega^2(r_{ax} + r_{bx})) \quad (18)$$

$$a_{cgy} = \frac{1}{2} \left(a_{ay} + a_{by} + \alpha(r_{ax} + r_{bx}) + \omega^2(r_{ay} + r_{by}) \right) \quad (19)$$

Since these equations rely on Equations (1) and (17), the uncertainties in Equations (1) and (17) propagate into the CoM accelerations. Following the methodology used to develop Equation (11), it can be shown that Equations (20) and (21) yield the uncertainties in the CoM accelerations.

$$\delta a_{cgx} = \frac{1}{2} \sqrt{\delta a_{ax}^2 + \delta a_{bx}^2 + \left(\frac{r_{ay} + r_{by}}{r_{ax} + r_{bx}} \right)^2 \delta \alpha^2 + 2 \left(\alpha^2 + (\omega^2)^2 \right) \delta r^2} \quad (20)$$

$$\delta a_{cgy} = \frac{1}{2} \sqrt{\delta a_{ay}^2 + \delta a_{by}^2 + \left(\frac{r_{ay} + r_{by}}{r_{ax} + r_{bx}} \right)^2 \delta \alpha^2 + 2 \left(\alpha^2 + (\omega^2)^2 \right) \delta r^2} \quad (21)$$

By examining Equations (20) and (21) we can observe that the uncertainties in the CoM accelerations can be minimized by selecting data from a pair of accelerometers that have opposite signed coordinates relative to the CoM. The uncertainties would be minimized most effectively by the accelerometers having coordinates of equal magnitudes and opposite signs since this would entirely eliminate the effect of the uncertainties in the angular acceleration. This suggests selection of accelerometers placed diagonal to one another.

Since Equations (18) and (19) depend not only on the relative position of the accelerometers, but also on their positions relative to the vehicle CoM, Equations (20) and (21) should consider uncertainty in the accelerometer positions due to uncertainty in locating the vehicle CoM. The vehicle CoM location rearward of the front axle is obtained with the following equation [9]:

$$d_f = \frac{W_R}{W_T} l \quad (22)$$

In Equation (22), d_f is the distance between the front axle and the CoM, W_R is the weight on the rear axle, W_T is the total vehicle weight, and l is the vehicle wheelbase. Following the methodology used throughout this paper, it can be shown that the uncertainty in d_f is given as follows:

$$\delta d_f = d_f \sqrt{\left(\frac{\delta W_R}{W_R} \right)^2 + \left(\frac{\delta W_T}{W_T} \right)^2 + \left(\frac{\delta l}{l} \right)^2} \quad (23)$$

After obtaining the CoM x and y accelerations and the yaw velocity, the vehicle velocity components in the vehicle-fixed coordinate system are obtained by integrating the following equations:

$$\frac{du}{dt} = a_{cgx} + v\omega \quad (24)$$

$$\frac{dv}{dt} = a_{cgy} - u\omega \quad (25)$$

In Equations (24) and (25), u is the vehicle's longitudinal velocity and the v is its lateral velocity. Using the Trapezoid Rule to perform the integration of these equations yields Equations (26) and (27).

$$u_t = u_{t-\Delta t} + \frac{\Delta t}{2} \left[(a_{cgx} + v\omega)_{t-\Delta t} + (a_{cgx} + v\omega)_t \right] \quad (26)$$

$$v_t = v_{t-\Delta t} + \frac{\Delta t}{2} \left[(a_{cgy} - u\omega)_{t-\Delta t} + (a_{cgy} - u\omega)_t \right] \quad (27)$$

Equation (28) gives the uncertainty in Equation (26) and Equation (29) gives the uncertainty in Equation (27).

$$\delta u_t = \delta u_{t-\Delta t} + \frac{\Delta t}{2} \sqrt{\delta a_{cgx,t-\Delta t}^2 + \delta a_{cgx,t}^2 + (\omega_{t-\Delta t})^2 \delta v_{t-\Delta t}^2 + (\omega_t)^2 \delta v_t^2 + v_{t-\Delta t}^2 (\delta \omega_{t-\Delta t})^2 + v_t^2 (\delta \omega_t)^2} \quad (28)$$

$$\delta v_t = \delta v_{t-\Delta t} + \frac{\Delta t}{2} \sqrt{\delta a_{cgy,t-\Delta t}^2 + \delta a_{cgy,t}^2 + (\omega_{t-\Delta t})^2 \delta u_{t-\Delta t}^2 + (\omega_t)^2 \delta u_t^2 + u_{t-\Delta t}^2 (\delta \omega_{t-\Delta t})^2 + u_t^2 (\delta \omega_t)^2} \quad (29)$$

Once the vehicle velocity components have been obtained in the vehicle-fixed coordinate system, the following equation can be used to transform them into the inertial coordinate system:

$$V_x = u \cdot c\theta - v \cdot s\theta \quad (30)$$

$$V_y = u \cdot s\theta + v \cdot c\theta \quad (31)$$

In Equations (30) and (31), $c\theta = \cos\theta$ and $s\theta = \sin\theta$. The uncertainty in the inertial frame velocities can be written as follows:

$$\delta V_x = \sqrt{c^2\theta \cdot \delta u^2 + s^2\theta \cdot \delta v^2 + (u \cdot s\theta + v \cdot c\theta)^2 \cdot \delta \theta^2} \quad (32)$$

$$\delta V_y = \sqrt{s^2\theta \cdot \delta u^2 + c^2\theta \cdot \delta v^2 + (u \cdot c\theta - v \cdot s\theta)^2 \cdot \delta \theta^2} \quad (33)$$

Now, the vehicle's change in velocity can be calculated using the following equations:

$$\Delta V_{x,t} = V_{x,t} - V_{x,0} \quad (34)$$

$$\Delta V_{y,t} = V_{y,t} - V_{y,0} \quad (35)$$

$$\Delta V_t = \sqrt{\Delta V_{x,t}^2 + \Delta V_{y,t}^2} \quad (36)$$

The uncertainties in the ΔV components and the overall ΔV are then given by the following equations:

$$\delta \Delta V_{x,t} = \delta V_{x,t} \quad (37)$$

$$\delta \Delta V_{y,t} = \delta V_{y,t} \quad (38)$$

$$\delta \Delta V_t = \sqrt{\left(\frac{\partial \Delta V_t}{\partial \Delta V_{x,t}}\right)^2 \delta \Delta V_{x,t}^2 + \left(\frac{\partial \Delta V_t}{\partial \Delta V_{y,t}}\right)^2 \delta \Delta V_{y,t}^2} \quad (39)$$

Evaluating the integrals within Equation (39) and substituting in Equations (37) and (38) yields the following equation:

$$\delta \Delta V_t = \frac{1}{\Delta V_t} \sqrt{\Delta V_{x,t}^2 \delta V_{x,t}^2 + \Delta V_{y,t}^2 \delta V_{y,t}^2} \quad (40)$$

NHTSA TEST #5257

As a specific example, consider NHTSA Test #5257, an NCAP side impact test involving a 2005 Ford Mustang Coupe. In this test, a moving deformable barrier (MDB) impacted the driver's side of the stationary Mustang at 38.4 mph (61.8 kph) with a heading of 90 degrees relative to the Mustang and with the velocity direction and wheels crabbed at 27 degrees relative to the MDB heading. The area of the Mustang that was contacted by the barrier began just rearward of the left front wheel well and terminated in the area of the B-pillar. Figure 2 is a series of images from the test video depicting the collision dynamics and Figure 3 is a graphic reproduced from the test report that depicts the impact configuration.

The Mustang was instrumented with three tri-axial accelerometers that were isolated from the crushing region of the vehicle – at the right front sill, the right rear sill, and the trunk floor. As shown previously, the sensitivity to uncertainties can be minimized by selecting the accelerometer combination with the maximum distance separating the accelerometers. In this instance, the maximum separation distance was obtained by using the right front sill and the trunk floor accelerometers and, thus, our analysis of the Mustang rotation relied on this combination. The MDB was instrumented with tri-axial accelerometers in the area of the MDB CoM and on the MDB frame in the area of the left rear wheel.

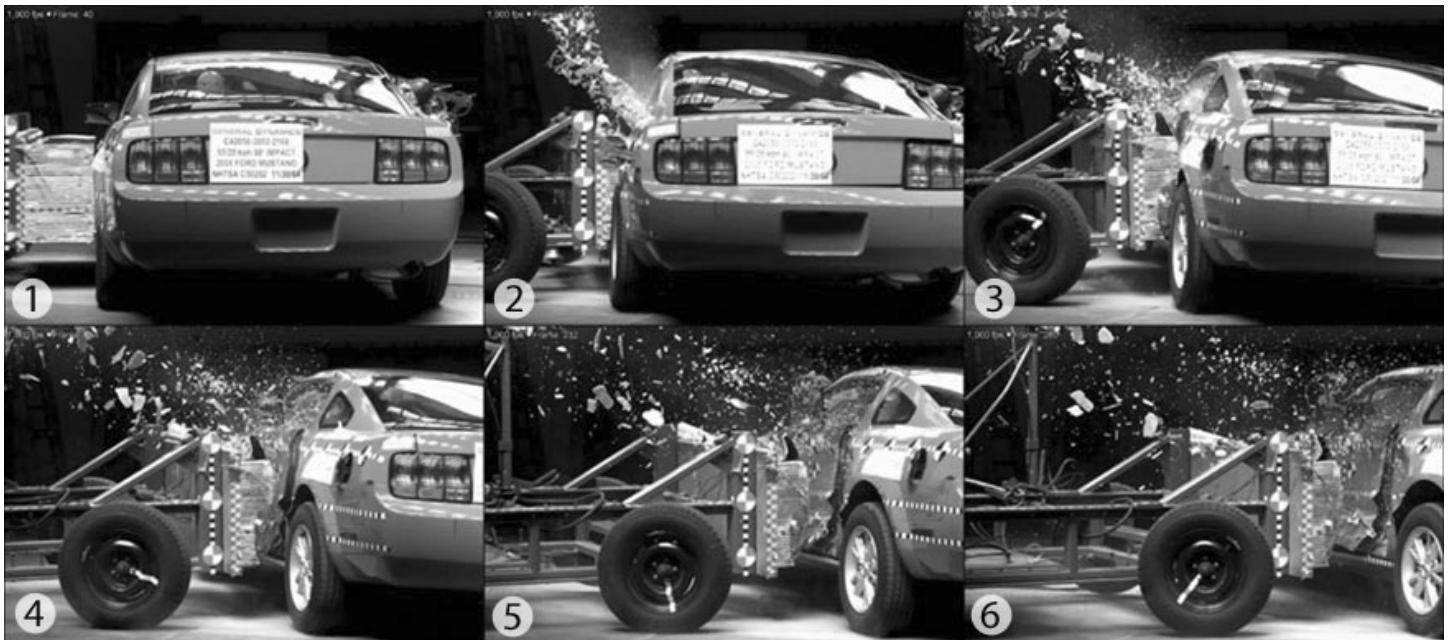


Figure 2 – NHTSA Test #5257, 2005 Ford Mustang, Side Impact Protection Test

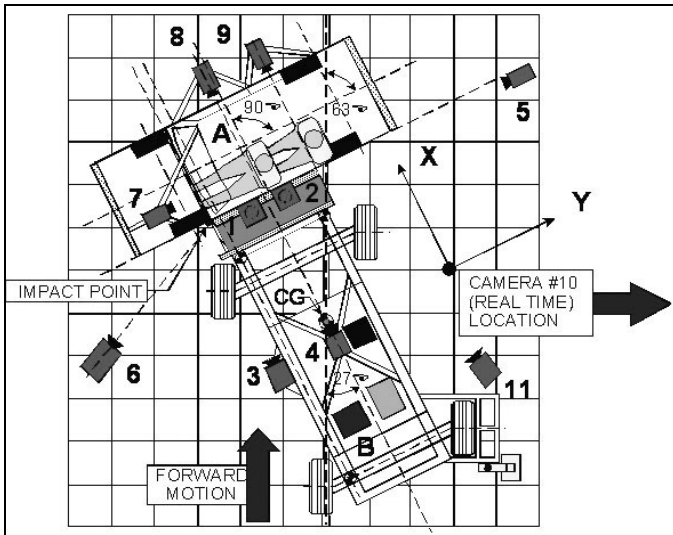


Figure 3 – NHTSA Test #5257, Impact Configuration

Longitudinal and lateral acceleration signals were obtained for these accelerometers and, after filtering, they were used in conjunction with the previously described equations to calculate each vehicle's angular velocity, heading, CoM accelerations, and velocity change throughout the duration of the impact. To estimate the uncertainty in this analysis, it is necessary to estimate the uncertainties in both the accelerometer locations and the acceleration readings. Appendix A examines the magnitude of these uncertainties and concludes that the uncertainty in the accelerometer locations relative to the CoM is on the order of 4 millimeters and that the uncertainty in the acceleration readings is about 1.5% of the channel's full-scale value, with a confidence around 75%. The reader is referred to Appendix A for a full discussion and justification of these values.

This level of uncertainty in the accelerations was obtained with signals filtered with a CFC 60 filter. SAE J211-1 [10] recommends the use of a CFC 180 filter for acceleration signals that will be integrated to obtain velocity and displacement. However, the analysis reported in Appendix A resulted in the conclusion that the CFC 180 filter had too high a level of uncertainty to be useful for our analysis here. The analysis reported in Appendix A tested the effect of the filter class on the integrated results and found that using a CFC 60 filter produced integrated results very close to those obtained with the CFC 180 filter. Thus, using a CFC 60 filter significantly reduced the level of uncertainty in the signals and had little effect on the results of the integration.

Given these uncertainty levels, Figure 4 is a graph containing high-end, low-end and mid-range yaw velocity curves for the Mustang in Test #5257. The high-end and low end curves bracket the uncertainty in the yaw velocity with a confidence level around 75%. Figure 5 is a graph containing similar curves for the MDB.

Consistent with the implication of Equation (14), the uncertainty in the yaw velocities accrues as the integration of the angular acceleration progresses and, thus, the low-end and high-end yaw velocity curves become progressively farther apart.

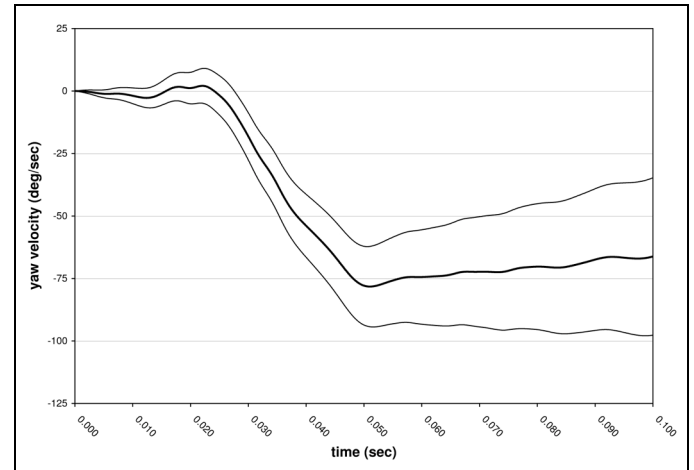


Figure 4 – Test #5257, Mustang Yaw Velocity Curves

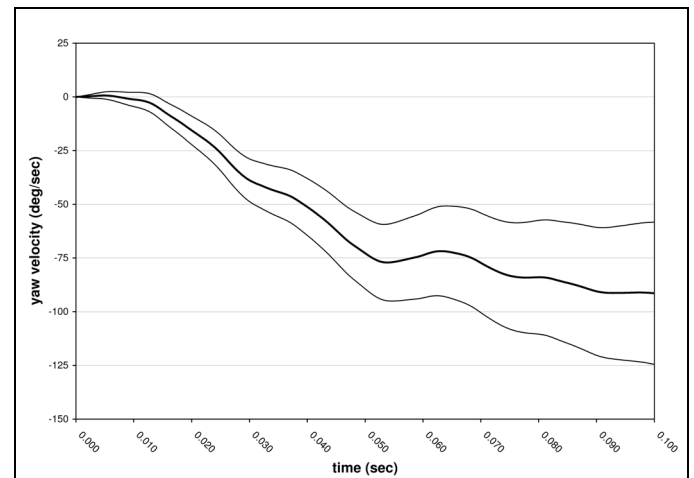


Figure 5 – Test #5257, MDB Yaw Velocity Curves

Figures 6 and 7 are graphs containing high-end, low-end and mid-range heading angle curves for the Mustang and the MDB, respectively. Again, the high-end and low-end curves bracket the uncertainty with a confidence level around 75%. Consistent with the implication of Equation (16), the uncertainty in the heading angle also accrues as the integration of the angular velocity progresses in time. In the case of the heading angle, this increase in uncertainty is due both to the integration process and to the progressively increasing uncertainty in the yaw velocity.

Figures 8 and 9 depict the resultant CoM accelerations for the Mustang and the MDB, respectively. The resultant acceleration on the Mustang approaches zero around 72 milliseconds and the resultant acceleration on the MDB approaches zero around 76 milliseconds.

Taking the average of these yields an impact duration of 74 milliseconds.

Figures 10 and 11 depict low and high-end velocity change curves for the Mustang and the MDB in this test.

Examination of Figures 4, 5, 10 and 11 reveals that after 74 milliseconds the vehicles had experienced the translational and rotational velocity changes given in Table 1. This table also gives the velocity directions of the vehicle centers of gravity after 74 milliseconds.

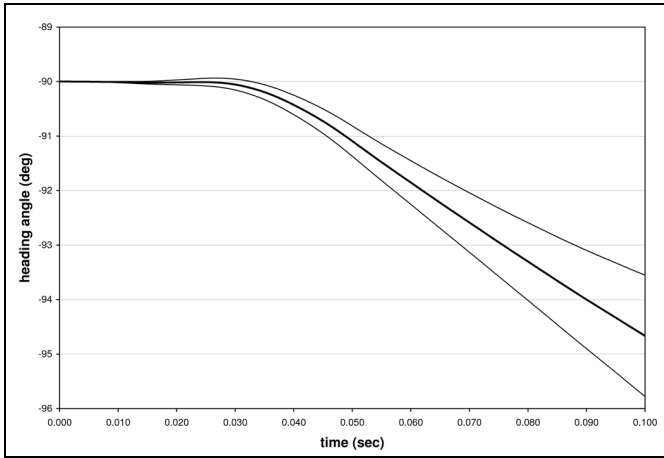


Figure 6 – Test #5257, Mustang Heading Angle Curves

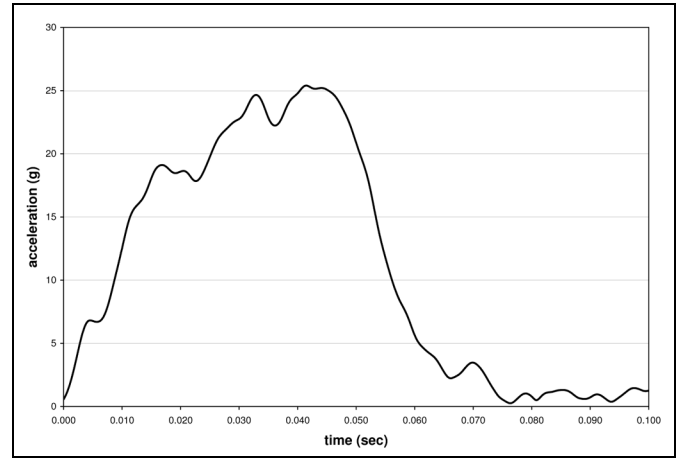


Figure 9 – Test #5257, MDB CoM Acceleration

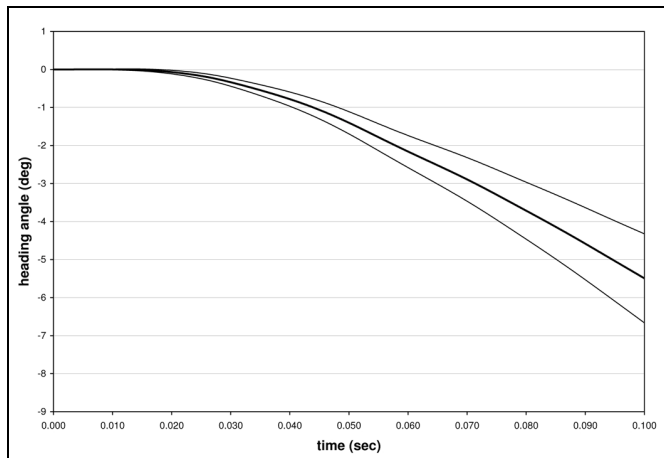


Figure 7 – Test #5257, MDB Heading Angle Curves

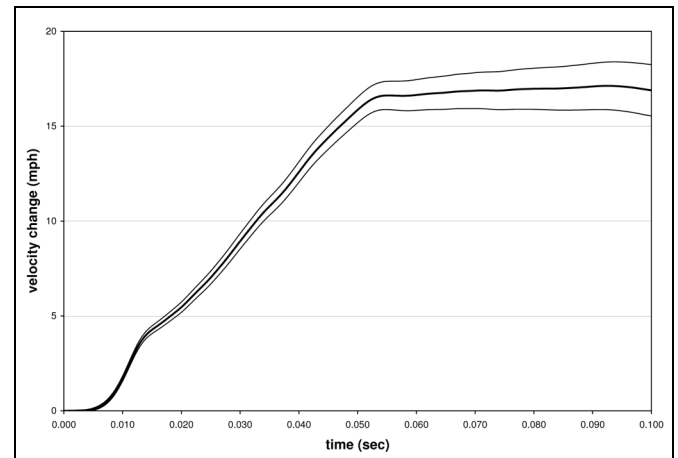


Figure 10 – Test #5257, Mustang ΔV

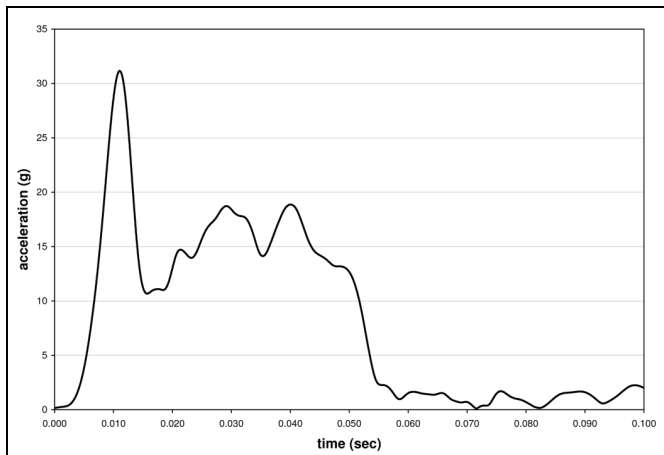


Figure 8 – Test #5257, Mustang CoM Acceleration

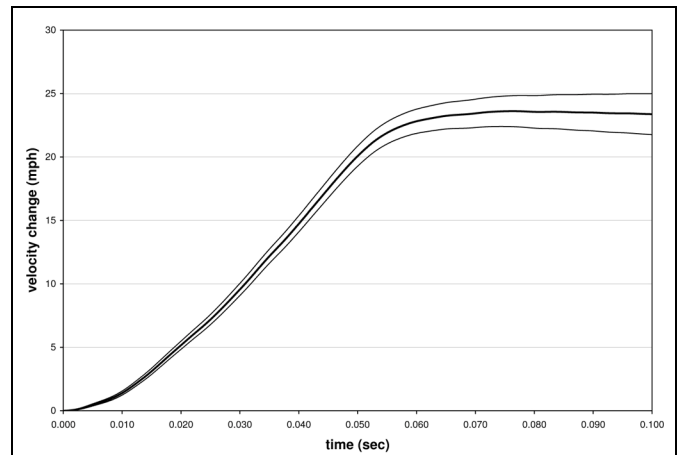


Figure 11 – Test #5257, MDB ΔV

$\Delta V_{\text{mustang}}$ (mph)	15.9 – 17.9
ΔV_{MDB} (mph)	22.4 – 24.8
Mustang $\Delta\omega$ (deg/s)	49 – 96
MDB $\Delta\omega$ (deg/s)	58 – 107
Mustang Departure Angle (deg)	79.6 – 76.4
MDB Departure Angle (deg)	40.0 – 50.0

Table 1 – Test #5257, Accelerometer Data Analysis Results

FITTING PIM SOLUTIONS TO THE DATA

Now that translational and rotational velocity changes for NHTSA Test #5257 have been obtained, this section describes a procedure that can be used to obtain the coefficient of restitution for this crash test. This procedure consists of fitting a planar impact mechanics solution to the translational and angular velocity changes obtained in the previous section. Reference 4 describes the equations of planar impact mechanics, which model a planar vehicle-to-vehicle impact using the principle of impulse and momentum. The reader is referred to this reference for a full treatment of these equations.

To perform the optimization, the analyst completes the following steps. First, the vehicle weights and dimensions are obtained from the test report. Dimensions of the pre-test, undamaged vehicle that are not given in the test report can be obtained from manufacturer specifications or from an exemplar vehicle.

Second, the vehicle yaw moments of inertia are calculated. For the analysis reported in this paper, these calculations were carried out using equations from

References 11 and 12. Next, vehicle specifications, photographs, and damage measurements from the crash test report are used to diagram the impact configuration for the test. Then, the impact center location is estimated and located relative to the vehicles' centers of mass. These locations include the lengths of lines connecting the impact center to the centers of gravity and the orientation of those lines relative to the vehicle headings. After that, the orientation of the intervehicular contact surface is estimated. An initial estimate of the coefficient of restitution and the impulse ratio are made and the equations of planar impact mechanics are used to calculate translational and angular velocity changes for the test.

Finally, to optimize the planar impact mechanics solution, the coefficient of restitution, the impulse ratio, and the location of the impact center are iteratively changed to minimize the error in matching the target translational and angular velocity changes determined from analysis of the accelerometer data. The error in the match is minimized using the method of least squares [5]. One planar impact mechanics solution should be optimized to match the low-end translational and rotational velocity change values from the accelerometer data analysis and another planar impact mechanics solution should be optimized to match the high-end velocity changes. This yields a range for the coefficient of restitution.

Consider this procedure for the specific case of NHTSA Test #5257. Figures 12 and 13 depict planar impact mechanics spreadsheets optimized for the high and low-end speed changes given in Table 2.

Mustang		MDB	
Inertial and Geometric Parameters			
3860	Weight (lb)	3004	
2681	Yaw Moment of Inertia (lb-ft-sec ²)	2086	
2.5	Distance from CG to Impact Center (IC) (ft)	6.4	
100	Angle Between Heading and CG-IC Line (deg)	23.0	
180	Heading Angle at Impact (deg)	63	
Initial Velocities			
0.0	Initial Translational Velocity (mph)	38.4	
0.0	Initial Yaw Velocity (deg/s)	0.0	
Final Velocities (mph)			
2.9	V_x	13.7	
16.5	V_y	13.1	
16.7	V	18.9	
Calculated Departure Angle (deg)			
80.0	Calculated Departure Angle (deg)	43.6	
79.6	Departure Angle from Accelerometer Data (deg)	40.0	
Calculated Change in Yaw Velocity (deg/s)			
49	Calculated Change in Yaw Velocity (deg/s)	58	
49	Yaw Velocity Change from Accelerometer Data (deg/s)	58	
Calculated Total Velocity Change (mph)			
16.7	Calculated Total Velocity Change (mph)	21.5	
15.9	Velocity Change from Accelerometer Data	22.4	
Impact Parameters			
Coefficient of Restitution		0.098	
Critical Impulse Ratio		-0.24	
Impulse Ratio (% of Critical)		74%	
Impulse Ratio		-0.18	
Contact Plane Orientation (deg)		90	
System Kinetic Energy (ft-lb)			
Initial		148016	
Final		74109	
Loss		73906	
Percent Energy Loss		49.9%	
Normal Direction Energy Loss		66457	
Tangential Direction Energy Loss		7450	
Least Squares Optimization			
Delta-d (ft)		0.060	
$Q_{\text{delta-V, Mustang}}$		85.5	
$Q_{\text{delta-V, MDB}}$		85.0	
$Q_{\text{yaw rate, Mustang}}$		0.0	
$Q_{\text{yaw rate, MDB}}$		0.0	
Q_{total}		170.5	

Figure 12 – NHTSA Test #5257, Low-End Planar Impact Mechanics Optimization

Mustang		MDB	
Inertial and Geometric Parameters			
3860	Weight (lb)	3004	
2193	Yaw Moment of Inertia (lb-ft-sec ²)	2086	
2.5	Distance from CG to Impact Center (IC) (ft)	6.4	
100	Angle Between Heading and CG-IC Line (deg)	23.0	
180	Heading Angle at Impact (deg)	63	
Initial Velocities			
0.0	Initial Translational Velocity (mph)	38.4	
0.0	Initial Yaw Velocity (deg/s)	0.0	
Final Velocities (mph)			
3.9	V _x	12.5	
18.2	V _y	10.8	
18.6	V	16.5	
Calculated Departure Angle (deg)			
78.0	Calculated Departure Angle (deg)	40.8	
76.4	Departure Angle from Accelerometer Data (deg)	50.0	
Calculated Change in Yaw Velocity (deg/s)			
75	Calculated Change in Yaw Velocity (deg/s)	85	
96	Yaw Velocity Change from Accelerometer Data (deg/s)	107	
Total Velocity Change (mph)			
18.6	Total Velocity Change (mph)	23.9	
17.9	Velocity Change from Accelerometer Data	24.8	
Impact Parameters			
	Coefficient of Restitution	0.216	
	Critical Impulse Ratio	-0.21	
	Impulse Ratio (% of Critical)	100%	
	Impulse Ratio	-0.21	
	Contact Plane Orientation (deg)	90	
System Kinetic Energy (ft-lb)			
	Initial	148016	
	Final	76249	
	Loss	71766	
	Percent Energy Loss	48.5%	
	Normal Direction Energy Loss	64628	
	Tangential Direction Energy Loss	7138	
Least Squares Optimization			
	Delta-d (ft)	0.065	
	Q _{delta-V, Mustang}	69.8	
	Q _{delta-V, MDB}	72.7	
	Q _{yaw rate, Mustang}	153.4	
	Q _{yaw rate, MDB}	152.9	
	Q _{total}	448.8	

Figure 13 – NHTSA Test #5257, High-End Planar Impact Mechanics Optimization

The low-end optimization resulted in a coefficient of restitution of 0.098 and the high-end a coefficient of restitution of 0.216. Thus, for Test #5257, we can state the coefficient of restitution as 0.157 ± 0.059 , implying that the coefficient of restitution in this case is certain to $\pm 38\%$ with a confidence around 75%. Within the optimizations depicted in Figure 12 and 13, we have considered an uncertainty of ± 6 pounds in the vehicle weights and $\pm 10\%$ in the vehicle yaw moments of inertia. This uncertainty level in the vehicle weight was calculated assuming four 1,500 pound capacity wheel scales with an uncertainty of 0.1% of full-scale. An uncertainty of 10% in the moments of inertia was judged to be a reasonable uncertainty level based on the discussion in References 11 and 12. The high-end moments of inertia generate the low-end coefficient of restitution and the low-end moments of inertia generate the high-end coefficient of restitution.

DISCUSSION

Equations (11), (14), (16), (20), (21), (23), (28), (29), (32), (33) and (40) provide general equations for quantifying the uncertainties that propagate through the analysis of accelerometer data for a vehicle-to-vehicle crash test. These equations specifically consider uncertainties associated with the physical location of the accelerometers and with the acceleration readings from those accelerometers. In the specific crash test considered here, NHTSA Test #5257, it was estimated that there was approximately 4 mm of uncertainty associated with the accelerometer locations and that the uncertainty in the acceleration readings was around 1.5% of the full-scale value of each channel. These uncertainties resulted in around 6% of uncertainty in the magnitude of the velocity changes and around 34% uncertainty in the yaw velocities. When these levels of uncertainty were then carried into the planar impact mechanics analysis, the resulting coefficient of restitution had an uncertainty of approximately $\pm 38\%$. Further

research would be necessary to say whether or not these levels of uncertainty are typical for this type of analysis.

The uncertainty in the coefficient of restitution could be reduced by using alternative methods to measure the change in translational and angular velocity that each vehicle experiences during the impact. For instance, the vehicle yaw velocities could be directly measured with an angular rate sensor [13]. Since much of the uncertainty in the angular velocity determined from translational acceleration data arises during integration of calculated angular accelerations, direct measurement of the angular velocity would eliminate much of this uncertainty.

Another alternative, would be to determine the vehicle yaw rates using video analysis or motion tracking techniques. These techniques would involve direct measurement of the vehicle yaw angles from which the yaw velocities would be calculated. Such a process would not accrue uncertainty in the manner that the integration of angular acceleration does. In principle, video analysis could also be used to obtain the CoM velocity changes and post-impact travel directions, and again, would not be subject to the uncertainty accrual that occurs with numerical integration. Of course, these techniques have their own set of uncertainties that would need to be explored and quantified.

CONCLUSIONS

- Equations (11), (14), (16), (20), (21), (23), (28), (29), (32), (33), and (40) provide a means for quantifying the uncertainty that accrues in the analysis of accelerometer data.
- Relevant uncertainties in this analysis include uncertainties associated with the accelerometer

locations and readings. Analysis of these uncertainties results in a range of values for the translational and rotational velocity changes that occur during the impact.

- The analysis of accelerometer data is more sensitive to uncertainties in the accelerometer readings than to uncertainties in the accelerometer positions.
- The effects of these uncertainties can be minimized by maximizing the distance between accelerometers and by using accelerometers that are placed diagonal to one another.
- The analysis reported in Appendix A resulted in the conclusion that the magnitude of the uncertainty in the acceleration readings for a typical crash test would be approximately 1.5% of the channel's full-scale value.
- Using the method of least squares, a low-end and high-end planar impact mechanics solution can be fit to the range of velocity changes obtained from the accelerometer data analysis. This results in a range of values for the coefficient of restitution for the crash test.
- In the specific case considered in this paper (NHTSA Test #5257), the coefficient of restitution had a range of $\pm 38\%$, with a confidence of 75%. Further research would be necessary to determine whether this range is typical.

REFERENCES

1. Bundorf, R. Thomas, "Analysis and Calculation of Delta-V from Crash Test Data," 960899, SAE, Warrendale, PA, 1996.
2. Marine, Micky C., et al., "Delta-V Analysis from Crash Test Data for Vehicles with Post-Impact Yaw Motion," 980219, SAE, Warrendale, PA, 1998.
3. Wirth, Jeffrey L., et al., "An Analysis of a Staged Two-Vehicle Impact," 2000-01-0464, SAE, Warrendale, PA, 2000.
4. Brach, Raymond M., Brach, R. Matthew, Vehicle Accident Analysis and Reconstruction Methods, SAE, ISBN 0-7680-0776-3, Warrendale, PA, 2005.
5. Brach, Raymond M., "Least Squares Collision Reconstruction," 870429, SAE, Warrendale, PA, 1987.
6. Brach, Raymond M., Dunn, Patrick F., Uncertainty Analysis for Forensic Science, Lawyers and Judges Publishing Company, ISBN 1-930056-20-6, Tucson, AZ, 2004.
7. Mandel, John, The Statistical Analysis of Experimental Data, Dover Publications, ISBN 0-486-64666-1, New York, 1984.
8. Taylor, John R., An Introduction to Error Analysis, University Science Books, ISBN 0-935702-75-X, Sausalito, CA, 1997.
9. Mango, Nicholas, "Measurement & Calculation of Vehicle Center of Gravity Using Portable Wheel Scales," 2004-01-1076, SAE, Warrendale, PA, 2004.
10. Surface Vehicle Recommended Practice J211-1, "(R) Instrumentation for Impact Test – Part 1 – Electronic Instrumentation," SAE, Warrendale, PA, 2003.
11. Allen, R. Wade, et al., "Estimation of Passenger Vehicle Inertial Properties and Their Effect on Stability and Handling," 2003-01-0966, SAE, Warrendale, PA, 2003.
12. MacInnis, Duane D., "A Comparison of Moment of Inertia Estimation Techniques for Vehicle Dynamics Simulation," 970951, SAE, Warrendale, PA, 1997.
13. Chou, Clifford C., Amin, Mukesh, "A Review of State-of-the-Art of Angular Rate Sensors," 2000-01-2668, SAE, Warrendale, PA, 2000.
14. U.S. Department of Transportation, National Highway Traffic Safety Administration Laboratory Test Procedure for FMVSS No. 214 "Dynamic" Side Impact Protection, January 1, 2003.
15. Sill, Robert D., "Minimizing Measurement Uncertainty in Calibration and Use of Accelerometers," Technical Paper 299, Endevco.

APPENDIX A – QUANTIFYING THE UNCERTAINTIES

Uncertainty in the Accelerometer Locations: NHTSA's Laboratory Test Procedure for FMVSS 214 tests requires the test facility to measure the location of the accelerometers to an accuracy of ± 3 mm (0.12 inches) [14]. NHTSA also requires their contractors to use wheel scales that are accurate to within 0.1% of full-scale. Considering these requirements and assuming first, that the test facility used 1,500 pound capacity scales, and second, that the wheelbase can also be measured to

within 3 mm, Equation (23) allows us to conclude that, for NHTSA Test #5257, there would be approximately 3 mm of uncertainty in the CoM location relative to the front axle. So, when located relative to the vehicle CoM, the accelerometer locations have approximately 3 mm of uncertainty from measuring their location and an additional 3 mm of uncertainty from locating the position of the vehicle's CoM. Since these are independent measurements, these uncertainties can be combined in quadrature, resulting in an expected uncertainty level in locating the accelerometer relative to the CoM of around 4 mm.

Uncertainty in Accelerometer Readings: To understand the level of uncertainty that exists in a typical acceleration signal, this section considers the following question: *If two accelerometers were mounted at an identical location on a crash test vehicle, how much difference would their acceleration readings exhibit?*

To answer this question, the authors examined accelerometer signals from the series of full-overlap frontal barrier impact tests listed in Table A1. The vehicles in these tests were each instrumented with left and right accelerometers that were mounted in the same longitudinal and vertical area of the vehicle, usually at the rear seat crossmember. Because the vehicles in these tests experienced little to no yaw rotation during the impact, these accelerometer combinations would theoretically yield redundant acceleration measurements that would only differ due to random measurement errors. This is, of course, an idealization since the accelerometers are not actually mounted at the same location on the vehicle. In reality, one would always expect some real difference in the left and right side accelerations due to factors other than random measurement errors. For instance, the following mechanisms would cause a real difference to exist between the left and right accelerations measured by the accelerometers [15]:

- Localized Deformation or Vibration at an Accelerometer Mounting Location
- Slight Yaw Rotation of the Test Vehicle
- A Discrepancy between the Longitudinal and Vertical Coordinates of the Accelerometers
- Insufficient Mechanical Connection between an Accelerometer and the Vehicle
- Misalignment of an Accelerometer Relative to the Vehicle

For the tests listed in Table A1, statistical analysis was conducted of the differences that existed between the left and right side acceleration signals, treating them as if they were truly redundant measurements of the vehicle accelerations. This was done with the expectation that this analysis would overestimate the degree to which random measurement errors would cause differences

between two truly redundant acceleration signals. For each of these tests, the authors conducted the following analysis:

- Longitudinal acceleration signals were obtained from accelerometers mounted in the same longitudinal area of the vehicle. Generally, these accelerometers were mounted in the area of the rear seat crossmember.
- Each signal was filtered with both a Class 60 and a Class 180 Butterworth filter. SAE J211-1 recommends the use of a Class 180 filter for acceleration readings that will be integrated to obtain velocity and displacement. However, as this analysis will show, the filter class significantly influences the level of uncertainty that exists in the acceleration signals. Thus, all of the analysis of the tests in Table 1 was carried out with signals obtained from both a Class 60 and a Class 180 filter with the intent of assessing the effect of the filter class on the level of uncertainty.
- For each test, the following calculations were carried out with both sets of filtered acceleration signals. This analysis was conducted over the period of time from when the vehicle first contacted the barrier until the vehicle separated from the barrier:
 - The normalized peak acceleration was calculated to determine the extent to which the channels' full-scale ratings were being utilized. This value is the peak acceleration divided by the average full-scale value.
 - The standard deviation between the acceleration signals was calculated at each time step. These standard deviations were then normalized with the average full-scale value for the two channels and then the average normalized standard deviation was calculated for the crash pulse.
 - The difference between the acceleration readings at each time step was calculated. These differences were then normalized using the average full-scale value for the two channels and the average and standard deviation of the normalized differences was calculated.

Table A1 lists the results of these calculations. The first two columns of this table give the test number and the vehicle make and model. The third column reports the average full scale value for the acceleration channels under consideration in each test. The fourth and seventh columns of the table report the normalized peak acceleration values for the signals obtained with the CFC 60 and CFC 180 filters, respectively. These values, which indicate the extent to which the full-scale range of the channels was utilized, ranged between 8 and 66

percent for the CFC 60 filter and between 9 and 69 percent for the CFC 180 filter. Thus, none of the accelerations recorded during these tests approached full utilization of the channels' capacities.

The fifth and eighth columns of Table A1 report the average normalized standard deviation for the acceleration signals filtered with the CFC 60 filter and CFC 180 filter, respectively. These standard deviations allow for meaningful comparison of the level of variability between the signals that result from the two filter classes. However, they do not provide a meaningful quantification of the level of uncertainty in the signals. Because they are calculated with only 2 samples, a range of \pm one standard deviation would only have a confidence level of around 50% [6]. In addition to that, the average value of the acceleration, in reference to which the standard deviation is calculated, also has a relatively low confidence level, given that it too was obtained with a sample size of only 2.

From the standpoint of quantifying the uncertainty, it seems best to simply determine the degree to which two redundant accelerometer signals typically differ from one another. This would give us a measure of level of uncertainty in the acceleration measurements from a single accelerometer. Thus, the sixth and ninth columns of Table A1 report the normalized averages and standard deviations of the difference between the two signals. Percentages listed in parenthesis represent confidence levels. For instance, for Test #5259, the CFC 60 filter produced acceleration signals that, on average, differed by 0.46% of full scale. Approximately 68 percent of the time, the difference between the signals would fall within 1.09% of that average value. Since, within our uncertainty analysis, we will assume that the difference between redundant measurements of the same acceleration could be either positive or negative, it makes sense to specify a certainty range centered on zero. Thus, in addition to the mean and standard deviation, the sixth and ninth columns also contain an additional certainty range that is centered on zero. The boundaries of these additional certainty ranges are defined by the addition of the average difference and one standard deviation from the average. In the case of Test #5259, the mean and standard deviation define a range between -0.63% and 1.55%. To obtain a range that is centered on zero, we specified a new certainty range between -1.55% and 1.55%. Approximately 81% of the differences between the two signals fall within this range.

As Table A1 shows, there were two tests for which the full scale values were not reported. Since random measurement errors should be a function of this full-scale value, these tests were not considered. In all of the other cases, the CFC 60 filter produced acceleration signals with less variability and higher confidence levels than the CFC 180 filter. Thus, from a certainty

standpoint, the CFC 60 filter is preferable. Since SAE J211-1 recommends the use of a CFC 180 filter for signals that will be integrated to obtain velocity and displacement, it is necessary to consider the difference in velocity and displacement that would result from the use of the two different filter classes.

Table A2 addresses this issue, reporting the difference between the velocity and displacement obtained with the signals from the two filter classes. These differences were examined at the time the vehicles separated from the barriers, denoted by the time at which the average acceleration went to zero. Since the average acceleration signals determined with the different filter classes went to zero at slightly different times, Table A2 also reports the difference in the apparent impact duration between the signals resulting from the different filter classes. For the analysis reported in Table A2, the integration of the acceleration signals to obtain velocity and displacement was carried out using the trapezoid rule. As Table A2 shows, the filter class had only a small effect on the ultimate value of the velocity, displacement and impact duration.

After calculating the normalized difference between the acceleration signals for the tests listed in Table A1, these values were pooled to test the degree to which the differences between the accelerometer signals in these tests could be characterized as random measurement errors that would be proportional to the channels' full-scale values. This analysis excluded the tests for which the full-scale value was not reported and Test #5677, which exhibited a variability that far exceeded that of the other tests listed in Table A1. The high level of variability in the accelerometer signals for this test likely indicates the presence of a systematic error in one of the signals such that the left and right signals cannot be considered redundant acceleration measurements.

Figure 14 is histogram displaying the results of pooling the normalized acceleration differences from the remaining tests. This histogram does tend towards a normal distribution with a mean acceleration difference of 0.22% and a standard deviation of approximately 1.39%. This data is generally consistent with our assumption that the left and right accelerometer signals can be considered as redundant measurements that differ only due to random measurement errors. Were the left and right signals truly redundant, the mean value of the acceleration differences would tend toward zero. That the mean difference falls as close to zero as it does is, thus, an encouraging result in favor of our assumption. One could potentially conclude that the mean difference of 0.22% represents the degree to which the signals are not actually redundant, though this conclusion would benefit from a more extensive list of tests. At any rate, the data represented in Figure 4 can be used to state an overall uncertainty range for a typical acceleration signal. Centering this certainty range on

zero, this data indicates that redundant acceleration measurements would be expected to lie within 1.62% of zero around 75% of the time. Given that some of this

variability is due to the left and right signals not being truly redundant, the analysis in this paper used a slightly reduced uncertainty range of $\pm 1.5\%$.

NHTSA Test #	Vehicle Make, Model, and Year	Average Full Scale Value	Maximum Acceleration as a Percentage of Full Scale, CFC 60	Average Standard Deviation as a Percentage of Full Scale, CFC 60	Certainty Range for Difference between Left and Right Signals, CFC 60	Maximum Acceleration as a Percentage of Full Scale, CFC 180	Average Standard Deviation as a Percentage of Full Scale, CFC 180	Certainty Range for Difference between Left and Right Signals, CFC 180
5259	2005 Ford Mustang	99 g	33.8%	0.66%	0.46% \pm 1.09% (68%) 0.00% \pm 1.55% (81%)	36.7%	2.18%	0.23% \pm 3.09% (68%) 0.00% \pm 3.32% (72%)
5611	2006 Toyota RAV4	861 g	8.2%	0.38%	0.25% \pm 0.62% (68%) 0.00% \pm 0.87% (80%)	9.0%	0.57%	0.27% \pm 1.30% (68%) 0.00% \pm 1.57% (76%)
5613	2006 Nissan Frontier	251 g	19.0%	0.92%	0.78% \pm 1.48% (68%) 0.00% \pm 2.26% (82%)	24.6%	1.39%	0.73% \pm 3.15% (68%) 0.00% \pm 3.88% (77%)
5615	2007 Chevrolet Tahoe	Full Scale Value Not Reported	Full Scale Value Not Reported	Full Scale Value Not Reported	Full Scale Value Not Reported	Full Scale Value Not Reported	Full Scale Value Not Reported	Full Scale Value Not Reported
5661	2007 Dodge Caliber	Full Scale Value Not Reported	Full Scale Value Not Reported	Full Scale Value Not Reported	Full Scale Value Not Reported	Full Scale Value Not Reported	Full Scale Value Not Reported	Full Scale Value Not Reported
5664	2007 Honda Fit	183 g	23.6%	1.04%	0.04% \pm 2.05% (68%) 0.00% \pm 2.09% (68%)	26.1%	1.99%	0.02% \pm 5.51% (68%) 0.00% \pm 5.53% (68%)
5665	2006 Infiniti FX35	147 g	28.7%	0.83%	0.19% \pm 1.66% (68%) 0.00% \pm 1.85% (73%)	51.63%	2.88%	0.19% \pm 8.07% (68%) 0.00% \pm 8.26% (68%)
5675	2007 Toyota Camry	99 g	34.7%	0.77%	0.06% \pm 1.37% (68%) 0.00% \pm 1.43% (70%)	46.3%	2.21%	0.06% \pm 5.42% (68%) 0.00% \pm 5.48% (68%)
5676	2007 Chevrolet Suburban	54 g	65.99%	1.12%	0.73% \pm 2.14% (68%) 0.00% \pm 2.87% (74%)	68.58%	1.63%	0.73% \pm 4.50% (68%) 0.00% \pm 5.23% (74%)
5677	2007 Toyota Yaris	78 g	62.49%	2.78%	0.67% \pm 5.81% (68%) 0.00% \pm 6.48% (73%)	68.70%	4.45%	0.66% \pm 11.06% (68%) 0.00% \pm 11.75% (71%)
5681	2007 Toyota FJ Cruiser	351 g	12.55%	0.42%	0.09% \pm 0.76% (68%) 0.00% \pm 0.85% (73%)	17.55%	1.29%	0.09% \pm 2.98% (68%) 0.00% \pm 3.07% (69%)
Overall					0.00% \pm 1.62% (75%)			

Table A1

NHTSA Test #	Vehicle Make, Model, and Year	Separation Velocity Difference Between CFC 180 and CFC 60	Separation Displacement Difference Between CFC 180 and CFC 60	Difference in Impact Duration Between CFC 180 and CFC 60
5259	2005 Ford Mustang	0.02 mph	0.00 in	0.0 ms
5611	2006 Toyota RAV4	0.01 mph	0.08 in	1.0 ms
5613	2006 Nissan Frontier	0.02 mph	0.04 in	0.6 ms
5615	2007 Chevrolet Tahoe	0.04 mph	0.32 in	5.0 ms
5661	2007 Dodge Caliber	0.00 mph	0.05 in	0.5 ms
5664	2007 Honda Fit	0.08 mph	0.18 in	3.3 ms
5665	2006 Infiniti FX35	0.00 mph	0.16 in	1.8 ms
5675	2007 Toyota Camry	0.00 mph	0.09 in	0.9 ms
5676	2007 Chevrolet Suburban	0.00 mph	0.14 in	2.1 ms
5677	2007 Toyota Yaris	0.01 mph	0.05 in	0.6 ms
5681	2007 Toyota FJ Cruiser	0.01 mph	0.14 in	2.0 ms

Table A2

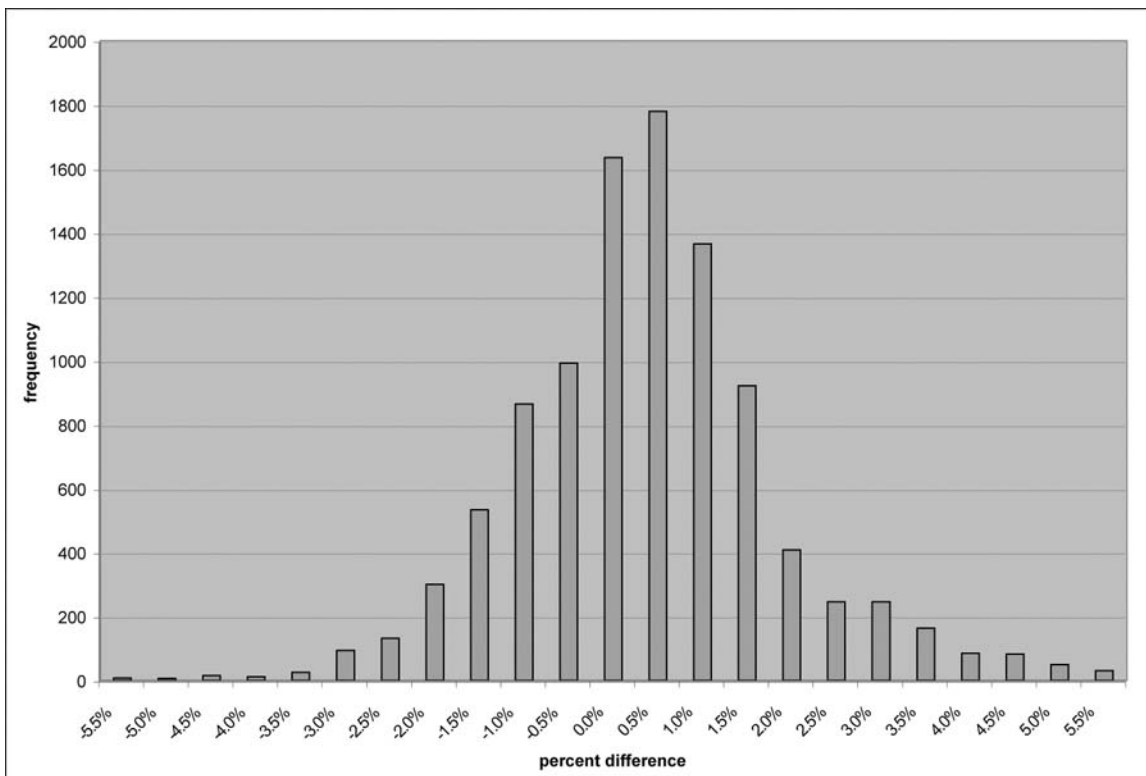


Figure 14 – Histogram Displaying Pooled Acceleration Differences